4. AN ASSESSMENT OF THE ROLE OF ANTHROPOGENIC CLIMATE CHANGE IN THE ALASKA FIRE SEASON OF 2015

James L. Partain Jr., Sharon Alden, Uma S. Bhatt, Peter A. Bieniek, Brian R. Brettschneider, Rick T. Lader, Peter Q. Olsson, T. Scott Rupp, Heidi Strader, Richard L. Thoman Jr., John E. Walsh, Alison D. York, and Robert H. Ziel

The 2015 Alaska fire season burned the second largest number of acres since records began in 1940. Human-induced climate change may have increased the risk of a fire season of this severity by 34%–60%.

Introduction. The 2015 Alaska fire season burned 5.1 million acres, the second largest burned area since 1940, exceeded only by the 2004 Alaska fire season when 6.2 million acres burned (Fig. 4.1a). Despite a below normal end-of-winter snowpack and an unseasonably warm spring with earlier snowmelt, which dried fuels early in the season, scattered showers and cool temperatures kept 2015 fire activity near normal through early June. During the first half of June, several days of maximum temperatures exceeded 30°C, relative humidity (RH) values were in the teens, and long daylight hours quickly dried surface and subsurface (duff) forest-floor fuels.

Beginning June 19, a period of vigorous thunderstorm activity resulted in an unprecedented weeklong lightning event with 36 000 strikes in three days. During this period, 65 000+ strikes in Alaska gave rise to nearly 270 ignitions of the preconditioned fuels. Burned acreage increased by 3.8 million acres (Fig. 4.1b) in the two and a half weeks following those starts (Fig. 4.1c). Lightning ignitions caused 99.5% of the acreage burned in Alaska in 2015. A westerly shift in upper-level winds by mid-July brought cool and damp weather that curtailed fire growth, and most extant fires burned little acreage after July 15.

This pattern highlights a significant difference between Alaska's top two fire seasons: 2004 burned significant acreage in July and again in August during extended warm and dry late summer weather, while 2015 saw the bulk of fire activity concentrated from mid-June to mid-July. These different pathways to large fire seasons demonstrate the importance of intraseasonal weather variability and the timing of dynamical features. Yet, underlying each case are the common requirements of: heat, extremely dry fuels, and ignition. One question that arises is whether the extremely warm and dry, yet convective, conditions of 2015 might be driven by anthropogenic climate change. This attribution study is a model-based test of the hypothesis that anthropogenic climate change increases the likelihood of fire seasons as extreme as 2015 through increasing flammability of fuels.

Measuring Fire Risk through the Buildup Index. This assessment uses the Buildup Index (BUI; Lawson and Armitage 2008), which is part of the Canadian Forest Fire Danger Rating System's Fire Weather Index system and represents potential fuel availability and flammability, based on cumulative scoring of daily temperature, relative humidity, and precipitation.

High BUI values generally represent periods of high fire danger (Ziel et al. 2015). BUI is often derived from meteorological station observations; however, gridded downscaled data (i.e., Bieniek et al. 2016) are used here because observations in Alaska are temporally and spatially spotty.

BUI is well suited for describing most fire seasons in northern boreal regions so is widely used by managers in Canada and Alaska. BUI begins to increase after the snowmelt, reaches its peak in June–July, and declines thereafter. Figure 4.2a displays BUI trends (April–September) for the Alaska boreal forest region (<600 m elevation) from 1979–2015. The BUI values represent the number of days (averaged over forest grids) that BUI exceeded 60, which marks the threshold for high fire danger in Alaska (Ziel et al. 2015). As an integrated metric, BUI effectively captures seasonal fire danger in Alaska, as per the large areas burned in 2004, 2015, and 2005. The exception is 2013, which, despite an extremely high BUI, had low fire activity because of few lightning strikes, highlighting ignitions as a necessary prerequisite for fires.

Modeling Wildfire Probability in Alaska. The attribution assessment was based on dynamical downscaling over the Alaska region by a regional model, the Advanced Research (ARW) version of the Weather Research and Forecasting (WRF) Model (Skamarock et al. 2008). An optimized configuration of the WRF model physical parameterizations for Alaska (Zhang et al. 2013) was employed. The downscaling covered a 262 x 262 grid-point domain that encompassed all of Alaska and portions of eastern Russia and northern Canada at 20 km spatial resolution with 49 vertical model levels. The European Centre for Medium-Range Weather Forecasts (ECMWF) interim reanalysis (ERA–Interim) data was downscaled for the 1979–2015 historical period (Bieniek et al. 2016), and a 60-year downscaling of the Geophysical Fluid Dynamics Laboratory Climate Model, version 3 (GFDL CM3) was completed to address the present climate and counterfactual (preindustrial) climate. Specifically, the GFDL CM3 was downscaled using WRF for a 60-year period (1986–2045) centered on 2015 based on historical (1986–2005) and RCP8.5 (2006–2045) simulations from CMIP5.

A 60-year subperiod (1986–2045) of a GFDL CM3 prescribed constant CO_2 (280 ppm) and aerosol concentrations (Donner et al. 2011) simulation represented the counterfactual or preindustrial world without anthropogenic climate change. Monthly difference fields between the two 60-year means
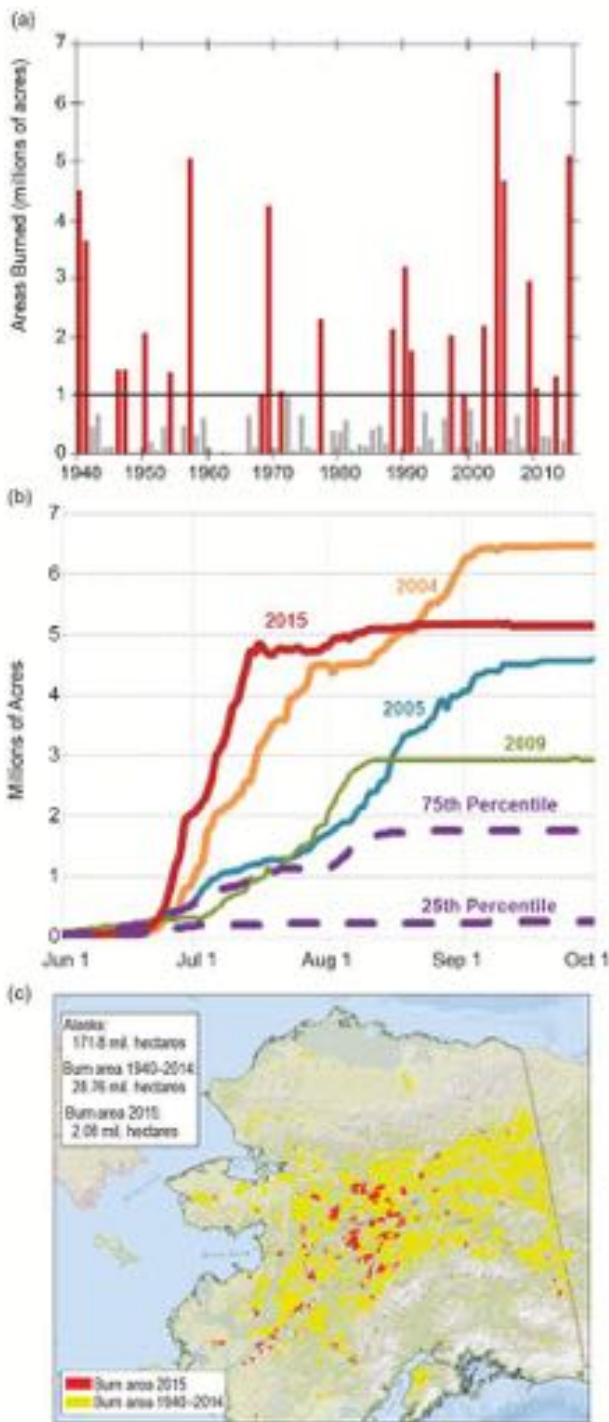
FIG. 4.1. (a) Annual time series of acres burned in Alaska and (b) averaged daily cumulative acres burned for specific high-fire years compared to the climatological 25th and 75th percentile (1994–2015) levels. The other above-75th percentile years of 1997 and 2002 are not shown for clarity because they lie close to the 75th percentile. (c) Displays fire perimeters for 2015 (red) and for the historical period of 1940–2014 (yellow). The area burned in 2015 is 7% of that which burned in the previous 75 years.
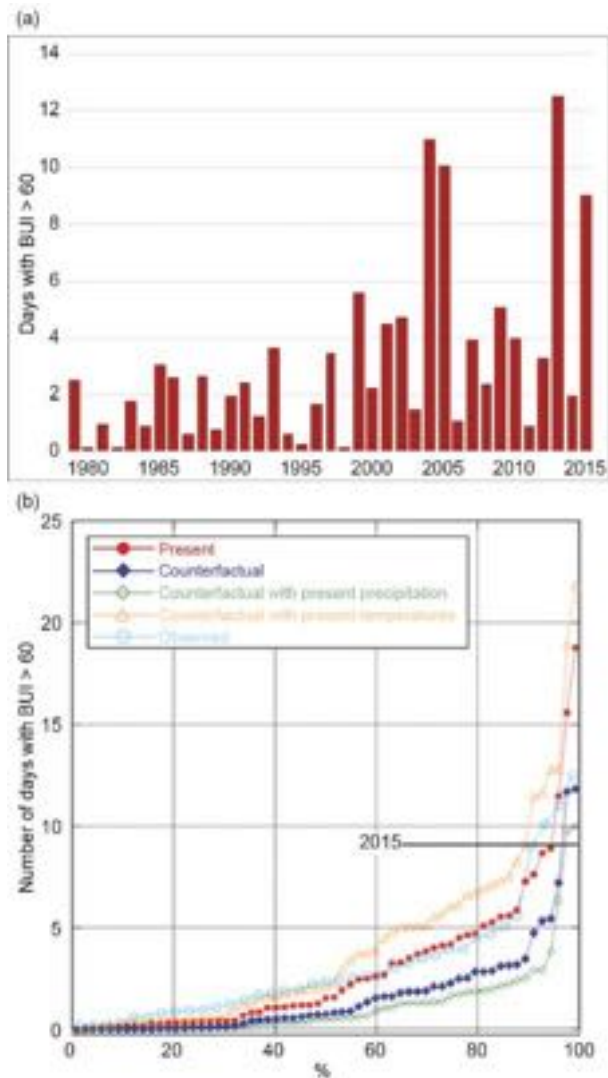
Fig. 4.2. (a) Number of days when the BUI index exceeds 60 when computed from the ERA-driven dynamical downscaling over the boreal forest region of Alaska and (b) cumulative frequency distribution of the number of days that BUI exceeds 60 when computed from the 1986–2045 GFDL-driven dynamical downscaling (red), the preindustrial (counterfactual) (blue), the 1986–2045 GFDL-driven downscaling in which only precipitation differs from the preindustrial (green), the 1986–2045 GFDL-driven downscaling in which only temperature differs from the preindustrial (orange), and observations based on the downscaled ERA–Interim reanalysis (cyan). The number of days of BUI greater than 60 for the 2015 fire season is marked on the plot with the horizontal black line and corresponds to approximately the 95th percentile of the model's present-day (present) distribution.

(present-day minus preindustrial) show that the spring–summer climate of Alaska has warmed (by 1°–3°C) and become wetter (2–10 mm mo^{-1} additional precipitation in May–July, with the largest increase in June, not shown). In nature, Alaska temperatures display a statewide warming of about 1°C in the annual mean and about 1.5°C in May–July since 1920; precipitation trends over the same period are mixed (Bieniek et al. 2014; see also NOAA's Climate at a Glance, www.ncdc.noaa.gov/cag). Possible reasons for differences in modeled-versus-observed trends in precipitation are discussed in the online supplemental material.

The model-derived differences were used to compute two 60-year time series of the BUI averaged over the Alaska boreal region from 1986–2045: one that included the influence of anthropogenic climate change [based on the original downscaled WRF output (i.e., using anthropogenic forcing)] and the other for the preindustrial control [based on the original downscaled WRF output adjusted by the differences between the GFDL monthly means for the two 60-year periods (i.e., not using anthropogenic forcing)]. The precipitation adjustment factors were the ratios of the two 60-year means to avoid negative values.

The GFDL-derived time series of BUI captures the observed (ERA–Interim) annual variability in BUI shown in Fig. 4.2a (comparison of observed BUI with GFDL BUI values not shown); however, the downscaled GFDL precipitation amounts are generally higher than the downscaled ERA–Interim for 1986–2015. Consequently, the downscaled GFDL BUI values were smaller than those obtained from downscaled ERA–Interim values. Therefore, all GFDL-derived BUI values were multiplied by 2.4, the ratio of the mean ERA-derived BUI for 1986–2015 to the corresponding GFDL-derived mean. This adjustment does not affect the percentile ranks that form the basis of our attribution assessment below.

Results. The anthropogenic contribution to the likelihood of a fire season of 2015's severity based on BUI was assessed using the fraction of attributable risk metric (Stott et al. 2004; National Academies 2016). Figure 4.2b shows the cumulative frequency distributions of the April–September integrated BUI values for observed and modeled scenarios. The 2015 observed value of nine days with BUI > 60, indicated by the black horizontal bar, was exceeded by 3 of 60 values (P_1 = 3/60 = 0.05) in the GFDL-simulated present climate (red) and by 2 of 60 values in the GFDL-simulated preindustrial (counterfactual) (dark blue) (P_o = 2/60 = 0.033), yielding a fraction of attributable risk to climate change of FAR = 1 − 0.033/0.050 = 0.34. Noting that two additional points

on the GFDL present-climate curve (red) are nearly identical to the 2015 observed value, an alternative estimate of FAR based on the number of years in which the 2015 value was essentially matched or exceeded (five) is FAR = 1 − 0.033/0.083 = 0.60. With the caveat that it is based on one ensemble member from one climate model, we conclude from this experiment that climate change has increased the risk of a fire year as severe as 2015 by 34%–60%.

Several sources of uncertainty are inherent in these estimates of increased risk of a severe fire season in Alaska. First, the sample size of events is small, as the number of fire years more severe than 2015 is 2 and 3 (for a total of 5) in the modeled preindustrial and the modeled present, respectively. Nevertheless, although there may be such uncertainty in the exceedance of the 2015 threshold, the results clearly indicate that the present climate (red line in Fig. 4.2b) has increased the risk of days with BUI > 60 relative to the preindustrial (dark blue line). Second, the results are based on only one model, GFDL CM3 (downscaled using WRF). While the GFDL model is one of the better-performing global models for Alaska (www.snap.uaf.edu/methods/models), simulated changes of temperature and precipitation since the preindustrial period vary among models. Third, our evaluation focused on an index (the BUI) of climate-driven potential for summer wildfire, not on the shorter-term weather variables of wind, humidity, and temperature that affect the rate of wildfire growth.

Sensitivity tests (orange and green lines) shown in Fig. 4.2b highlight the competing effects of temperature and precipitation as climate changes. If precipitation does not change within the model, the postindustrial warming increases the severity of the fire years in the upper half of the distribution (orange line). An increase of precipitation, in the absence of any temperature change, decreases the severity of the uppermost half of the distribution (green line). The impact of increased temperatures outweighs the impact of increased precipitation in the change from the preindustrial. For the future, annual average temperatures in Alaska are projected to increase by 1°C to 2°C above present values by 2050, while precipitation is projected to increase by 15%–30% by the end of the century (Chapin et al. 2014).

Conclusion. The 2015 fire season in Alaska was remarkable for its early-season total acres burned, which resulted from 1) fuel flammability due to the warm and dry conditions of May and June, and 2) lightning-induced ignitions in June. The rains of mid-summer likely prevented a new record for area burned in Alaska in 2015. An attribution analysis indicates that 2015's fuel conditions reached a level that is 34%–60% more likely to occur in today's anthropogenically changed climate than in the past. The major uncertainty in such an attribution assessment is the as-yet unknown relationship between climate change and the major lightning events that ignite widespread fires.

This study's conclusion is consistent with the similar finding by Yoon et al. (2015) for wildfires in California, where an increased wildfire risk relative to the preindustrial climate emerged in the 1990s. Similar model-derived results were found for the western United States (Luo et al. 2013; Yue et al. 2013), Canada (Flannigan et al. 2015), and Alaska (Young et al. 2016).

REFERENCES

Bieniek, P. A., J. W. Walsh, R. L. Thoman, and U. S. Bhatt, 2014: Using climate divisions to analyze variations and trends in Alaska temperature and precipitation. *J. Climate*, **27**, 2800–2818, doi:10.1175/JCLI-D-13-00342.1.

——, U. S. Bhatt, J. E. Walsh, T. S. Rupp. J. Zhang, J. Krieger, and R. Lader, 2016: Dynamical downscaling of ERA-Interim temperature and precipitation for Alaska. *J. Appl. Meteor. Climatol.*, **55**, 635–654, doi:10.1175/JAMC-D-15-0153.1.

Chapin, F. S., III, S. F. Trainor, P. Cochran, H. Huntington, C. Markon, M. McCammon, A. D. McGuire, and M. Serreze, 2014: Alaska. *Climate Change Impacts in the United States: The Third National Climate Assessment*, J. M. Melillo et al., Eds., 514–536, doi:10.7930/J00Z7150.

Donner, L. J., and Coauthors, 2011: The dynamical core, physical parameterizations, and basic simulation characteristics of the atmospheric component AM3 of the GFDL global coupled mdel CM3. *J. Climate*, **24**, 3484–3519, doi:10.1175/2011JCLI3955.1.

Flannigan, M. D., B. M. Wotton, G. A. Marshall, W. J. de Groot, J. Johnston, N. Jurko, and A. S. Cantin, 2015: Fuel moisture sensitivity to temperature and precipitation: Climatic change implications. *Climatic Change*, **134**, 59–71, doi:10.1007/s10584-015-1521-0.

Lawson, B. D., and O. B. Armitage, 2008: Weather guide for the Canadian forest fire danger rating system. Canadian Forest Service, 73 pp. [Available online at http://fire.ak.blm.gov/content/weather/2008%20CFFDRS%20Weather%20Guide.pdf.]

Luo, L. F., Y. Tang, S.-Y. Zhong, X. D. Bian, and W. E. Heilman, 2013: Will future climate favor more erratic wildfires in the western United States? *J. Appl. Meteor. Climatol.*, **52**, 2410–2417, doi:10.1175/JAMC-D-12-0317.1.

National Academies, 2016: *Attribution of Extreme Weather Events in the Context of Climate Change*. National Academies Press, 186 pp., doi:10.17226/21852.

Skamarock, W. C., and Coauthors, 2008: A description of the Advanced Research WRF version 3. NCAR Tech Note, NCAR/TN–475+STR, 113 pp. [Available online at www2.mmm.ucar.edu/wrf/users/docs/arw_v3.pdf.]

Stott, P., D. A. Stone, and M. R. Allen, 2004: Human contribution to the European heatwave of 2003. *Nature*, **432**, 610–614, doi:10.1038/nature03089.

Yoon, J. H., S.-Y.S. Wang, R. R. Gillies, L. Hipps, B. Kravitz, and P. J. Rasch, 2015: Extreme fire season severity in California: A glimpse into the future? [in "Explaining Extremes of 2014 from a Climate Perspective"]. *Bull. Amer. Meteor. Soc.*, **96** (**12**), S5–S9, doi:10.1175/BAMS-D-15-00114.1.

Young, A. M., P. E. Higuera, P. A. Duffy, and F. S. Hu, 2016: Climate thresholds shape northern high latitude fire regimes and imply vulnerability to future climate change. *Ecogeography*, in press doi:10.1111/ecog.02205.

Yue, X., L. J. Mickley, J. A. Logan, and J. O. Kaplan, 2013: Ensemble projections of wildfire activity and carbonaceous aerosol concentrations over the western United States in the mid-21st century. *Atmos. Environ.*, **77**, 767–780, doi:10.1016/j.atmosenv.2013.06.003.

Zhang, X., and Coauthors, 2013: Beaufort and Chukchi Seas Mesoscale Meteorology Modeling Study, final project report. Bureau of Ocean Energy Management Tech. Rep. BOEM 2013-0119, 204 pp. [Available online at www.boem.gov/BOEM-2013-0119/.]

Ziel, R. H., and Coauthors; 2015: Modeling fire growth potential by emphasizing significant growth events: characterizing climatology of fire growth days in Alaska's boreal forest. *11th Symp. on Fire and Forest Meteorology*, Minneapolis MN, Amer. Meteor. Soc., 1.2. [Available online at https://ams.confex.com/ams/11FIRE/webprogram/Paper272864.html.]

Table 28.1. Summary of Results

	ANTHROPOGENIC INFLUENCE ON EVENT		
	INCREASE	**DECREASE**	**NOT FOUND OR UNCERTAIN**
Heat	**Global Temperature** (Ch. 2) **South India & Sri Lanka** (Ch. 2) **Central Europe** (Ch. 11) **Europe** (Ch. 12) **Ethiopia and Southern Africa** (Ch. 15) **N.W. China** (Ch. 19) **W. China** (Ch. 20) **Japan** (Ch. 21) **Indonesia** (Ch. 22) **S. Australia** (Ch. 23) **Australia** (Ch. 24)		**Central Equitorial Pacific** (Ch. 2)
Cold		**Northeastern U.S.** (Ch. 7)	**Mid-South Atlantic U.S.** (Ch. 7) **N. America** (Ch. 8)
Heat & Humidity	**Egypt** (Ch. 14) **India & Pakistan** (Ch. 16)		
Dryness	**Indonesia** (Ch. 22) **Tasmania** (Ch. 25)		
Heavy Precipitation	**China** (Ch. 18)		**Nigeria** (Ch. 13) **India** (Ch. 17)
Sunshine	**United Kingdom** (Ch. 10)		
Drought	**Canada** (Ch. 9) **Ethiopia and Southern Africa** (Ch. 15)		
Tropical Cyclones	**Western North Pacific** (Ch. 26)		
Wildfires	**Alaska** (Ch. 4)		
Sea Ice Extent		**Arctic** (Ch. 27)	
HIGH TIDE FLOODS	**SOUTHEASTERN U.S.** (CH. 6)		
SNOWPACK DROUGHT	**WASHINGTON U.S.** (CH. 5)		
TOTAL	23	2	5

	METHOD USED			Total Events
Heat	Ch. 2: **CMIP5 modeling** Ch. 11: **Observations; weather@home modeling** Ch. 12: **HadGEM3-A modeling** Ch. 15: **CMIP5 modeling** Ch. 19: **CMIP5 modeling with ROF; FAR** Ch. 20: **CMIP5 modeling with ROF; FAR** Ch. 21: **MIROC5-AGCM modeling** Ch. 22: **Observations; CMIP5 modeling** Ch. 23: **weather@home modeling; FAR** Ch. 24: **BoM seasonal forecast attribution system and seasonal forecasts**			12
Cold	Ch. 7: **Observations; CMIP5 modeling** Ch. 8: **AMIP (IFS model) modeling**			3
Heat & Humidity	Ch. 14: **weather@home modeling** Ch. 16: **Non-stationary EV theory; C20C+ Attribution Subproject**			2
Dryness	Ch. 22: **Observations; CMIP5 modeling** Ch. 25: **Observations; Modeling with CMIP5 and weather@home**			2
Heavy Precipitation	Ch. 13: **Observations; Modeling with CAM5.1 and MIROC5** Ch. 17: **Observations; Modeling with weather@home, EC-Earth and CMIP5** Ch. 18: **HadGEM3-A-N216 modeling; FAR**			3
Sunshine	Ch. 10: **Hadley Centre event attribution system built on the high-resolution version of HadGEM3-A**			1
Drought	Ch. 9: **Observations; CMIP5 modeling; Trend and FAR analyses** Ch. 15: **CMIP5 modeling, land surface model simulations, and statistical analyses**			2
Tropical Cyclones	Ch. 26: **GFDL FLOR modeling; FAR**			1
Wildfires	Ch. 4: **WRF-ARW optimized for Alaska with metric of fire risk (BUI) to calculate FAR**			1
Sea Ice Extent	Ch. 27: **OGCM modeling**			1
HIGH TIDE FLOODS	Ch. 6: **TIDE-GAUGE DATA; TIME-DEPENDENT EV STATISTICAL MODEL**			1
SNOWPACK DROUGHT	Ch. 5: **OBSERVATIONS; CESM1 MODELING**			1
				30

ACRONYMS:

AMIP: Atmospheric Model Intercomparison Project

BoM: Bureau of Meteorology, Australia

BUI: Buildup Index

CAM: Community Atmosphere Model, http:www.cesm.ucar.edu

CESM: Community Earth System Model

CMIP: Coupled Model Intercomparison Project

FAR: Fraction of Attributable Risk

EC-EARTH: https://verc.enes.org/

EV: Extreme Value

GFDL FLOR: Geophysical Fluid Dynamics Laboratory Forecast version Low Ocean Resolution

GHCN: Global Historical Climatology Network

IFS: Integrated Forecast System

MIROC5–AGCM: Model for Interdisciplinary Research on Climate–Atmospheric General Circulation Model

OGCM: Ocean General Circulation Model

ROF: Regularized Optimal Fingerprinting

weather@home: http:www.climateprediction.net/weatherathome

WRF-ARW: Advanced Research (ARW) version of the Weather Research and Forecasting (WRF) model